RSC Pharmaceutics

ROYAL SOCIETY OF CHEMISTRY

PAPER

View Article Online
View Journal

Cite this: DOI: 10.1039/d5pm00345h

Development and evaluation of fenticonazole nitrate-loaded, fucoidan-coated lecithin–chitosan nanoparticles for the treatment of vaginitis

Valamla Bhavana,[a] Padakanti Sandeep Chary,[a] Urati Anuradha,[b] Kishan Kumar Parida,[b] Nitin Pal Kalia [b] and Neelesh Kumar Mehra *[a]

Received 19th November 2025,
Accepted 13th January 2026

DOI: 10.1039/d5pm00345h

rsc.li/RSCPharma

In this investigation, self-assembling fenticonazole-loaded lecithin–chitosan nanoparticles (FZNP) with cationic zeta potential were altered by coating them with an anionic fucoidan polymer (Fu-FZNP) through an ionic gelation method to overcome the vaginal mucosal barrier. FZNP and Fu-FZNP possessed particle sizes of 129.20 ± 0.25 nm and 227.10 ± 1.54 nm, polydispersity indexes of 0.21 ± 0.00 and 0.26 ± 0.01, and zeta potentials of 30.96 ± 1.15 mV and −26.75 ± 0.3 mV, respectively. The entrapment efficiency and drug loading were 65.47% ± 2.32% and 11.69% ± 0.414% for FZNP and 71.13% ± 5.74% and 7.41% ± 0.60% for Fu-FZNP, respectively. The nanoparticles exhibited spherical and smooth morphology under TEM imaging. An excised goat vagina was used for the *ex vivo* permeation studies, which showed drug permeations of 61.74% ± 2.07% for FZNP and 72.11% ± 1.4% for Fu-FZNP. FZNP and Fu-FZNP demonstrated antibacterial and antifungal properties against *Staphylococcus aureus* and *Candida albicans*, respectively, *in vitro*. Therefore, FZN and Fu-FZNP may be developed further for the safe, practical, and efficient treatment of mixed vaginal infections.

1. Introduction

Vaginal infection is a chronic gynecological issue in women of reproductive age that can lead to various health complications. Mixed vaginitis, which occurs rarely, is caused by the presence of two vaginal pathogens (bacterium and fungus (*Candida* species)), necessitating dual therapy with a combination of antifungal and antibacterial drugs or broad-spectrum monotherapy to eliminate concurrent symptoms.[1–3]

Fenticonazole is an imidazole derivative with antifungal properties that was created about thirty years ago to treat dermatomycosis and *Candida* vaginitis topically. Fenticonazole nitrate (FZN) has demonstrated extensive antimycotic action against yeasts and dermatophytes in both *in vitro* and clinical investigations.[4,5] Three distinct mechanisms allow fenticonazole to perform its specific antimycotic activity: (i) reduction of the protease acid secretion *of Candida albicans*, (ii) cytoplasmic membrane damage, and (iii) blockage of cytochrome oxidase and peroxidases.[3,6–9] Fenticonazole nitrate is commercially available in conventional dosage forms, such as vaginal creams, ovules, and pessaries (*e.g.*, 2% vaginal cream and 600 mg vaginal ovules), which are commonly prescribed for vulvovaginal candidiasis and mixed infections. However, these formulations suffer from limitations such as poor retention at the vaginal site and require frequent dosing, leading to reduced patient compliance.

Two additional pharmacological properties of fenticonazole are noteworthy. The drug persists in the skin's stratum corneum for a prolonged period, and it has unique pharmacokinetic properties that enable the accumulation of the active drug in mucosal tissue for up to 72 h. This accumulation forms a reservoir of FZN, delaying the need for consecutive administrations. Moreover, the assessment of fenticonazole plasma levels has validated the drug's inadequate systemic absorption. Consequently, for mixed infections comprising mycotic, bacterial, dermatophyte, and/or *Trichomonas* species, fenticonazole may be the perfect topical substitute for combination therapy.[10–12]

The vaginal route is an essential mode of drug delivery to treat local and systemic ailments. The vaginal route offers several benefits, including large surface area, adequate blood supply, lack of first-pass effect, slightly greater drug permeability, and self-insertion simplicity.[13] However, conventional vaginal dosage forms are limited by short residence time,

[a]*Pharmaceutical Nanotechnology Research Laboratory, Department of Pharmaceutics, National Institute of Pharmaceutical Education and Research (NIPER), Ministry of Chemicals and Fertilizers, Government of India, Hyderabad, Telangana, 500037 India. E-mail: neelesh@niperhyd.ac.in, neelesh81mph@gmail.com; Tel: +91-8839030437, +91-40-230747750*
[b]*Department of Biological Sciences, National Institute of Pharmaceutical Education and Research (NIPER), Hyderabad, Telangana, 500037 India*

mucus turnover, and variable drug retention, which can reduce therapeutic efficacy. The literature suggests using inventions that attach to vaginal mucosa by forming chemical and physical bonds with the mucus as one way to address these challenges. However, mucosal drug delivery is intrinsically challenging since vaginal medication distribution is constrained by the presence of anatomical and physiological factors.[14–16]

Many medical conditions, such as cancer and fungal and bacterial infections, can be treated and prevented through vaginal drug delivery.[17] The high porosity, negative charge, interconnectivity, and the hydrophilic and hydrophobic regions of the vaginal microenvironment contribute to the barrier properties of vaginal drug delivery. In order to enhance the vaginal delivery of active substances, mucoadhesive and mucus-penetrating particles have been designed by adjusting their chemical constituents, surface characteristics, size, and amount of surface functionalization.[18,19]

The advancement of nanotechnology in recent times has created novel pathways, *i.e.*, using muco-adhesive and mucus-penetrating polymers and zeta-potential-modifying polymers to overcome the vaginal mucosal barriers.[20–22] A naturally occurring polycationic polymer, chitosan, is created when chitin undergoes partial deacetylation. Chitosan has the added benefit of being naturally derived, which makes it biodegradable and biocompatible, with good bioadhesive properties.[23] Chitosan is being utilized to produce nanoparticles *via* ionotropic gelation with tripolyphosphate.[24,25] Furthermore, chitosan has been studied for the stabilization of microemulsions in combination with lecithin as an emulsifying agent.[26] Lecithin is a phospholipid combination that is commonly utilized to form liposomes and micelles.[27,28] Interestingly, encapsulating these lipid-based nanostructures with chitosan has been shown to improve their stability and give mucoadhesive properties.[29–31] In recent years, films and gels built around the bonding between negatively charged phospholipids and chitosan have been considered for the transport of lipophilic drugs.[32,33] Fucoidan is a sulfated polysaccharide with a high density of negatively charged sulfate groups, which plays a crucial role in modulating the surface charge (zeta potential) of lecithin–chitosan nanoparticles. This modulation reduces excessive mucoadhesion while promoting mucus penetration by minimizing the electrostatic interactions with negatively charged mucins. Additionally, fucoidan's bioactive properties, including anti-inflammatory and antimicrobial effects, further enhance its suitability for vaginal drug delivery.

The lecithin–chitosan nanoparticles are promising drug carriers formed by the supramolecular self-organizing electrostatic interactions between negatively charged lecithin and positively charged chitosan.[34–36] Chitosan/lecithin nanoparticles loaded with melatonin, quercetin, and diflucortolone valerate are just a few examples in this study.[37–40]

Mucus is digested, excreted, regenerated, and secreted continually. Mucus has a brief turnover time, frequently measured in minutes to hours, especially for the poorly adhering mucus layer. Effective particle clearance is achieved by the vaginal mucus output rate of about 6 mL day^{-1} for vaginal medication delivery. Therefore, there is a need to develop smart delivery schemes that do not initially interact with the mucus but later adhere to the membrane and mucus to overcome the continually cleared mucus.[41–43] To circumvent the drawbacks of available vaginal drug delivery systems while preserving and even refining the safety profiles, a novel vaginal drug delivery system was developed by surface modification of positively charged lecithin–chitosan nanoparticles with negatively charged fucoidan to alter the zeta potential of the system.

2. Materials and methods

2.1. Materials

Fenticonazole was obtained as a gift sample from Optimus Pharma, Hyderabad. Fucoidan and chitosan were purchased from Sigma-Aldrich, St Louis, Missouri, USA. The essential oils (lemongrass oil, lavender oil) were procured from Botanical Healthcare (Bangalore, India). Solvents such as methanol (HPLC analytical grade) were purchased from SRL Chemicals, India. Polyvinyl alcohol (98–99% hydrolysis) was purchased from Loba Chemie (Mumbai, India) and hyaluronic acid from PC CHEM, Mumbai, India. Deionized water was used for the studies, and other chemicals were used as received from the distributors.

2.2. Methodology

2.2.1. Preparation of fenticonazole nitrate lecithin–chitosan nanoparticles (FZNP). The novel antifungal formulation development involves the preparation of self-assembling nanoparticles, as shown in Fig. 1. The ethanol injection method based on the ionic interaction technique was exploited to prepare lecithin–chitosan nanoparticles. Initially, 0.2% chitosan (w/v) aqueous phase solution in 1% glacial acetic acid was placed on a magnetic stirrer (Remi, Mumbai) for 16 h (solution A). For nanoparticle preparation, FZN was solubilized in an ethanolic solution containing lecithin (solution B). In short, the formulation was acquired by swiftly injecting solution B from a syringe into solution A, which was stirred continuously at 500 ± 10 rpm on a magnetic stirrer. The various batches of the nanoparticles were formulated to develop stable formulations, as illustrated in Table 1.

2.2.2. Preparation of fenticonazole nitrate-loaded, fucoidan-coated lecithin–chitosan nanoparticles (Fu-FZNP). The nanoparticles prepared above, with positive zeta potential, were further coated with negatively charged fucoidan (Fu) to obtain zeta-potential-modified nanoparticles to overcome the interaction with the negatively charged mucus barrier, as shown in Fig. 1. Surface coating of nanoparticles with fucoidan was carried out by a post-fabrication adsorption method. Fucoidan was dissolved in deionized water, and an accurately measured volume of the nanoparticle suspension was added dropwise to the fucoidan solution to achieve a nanoparticle-to-fucoidan stoichiometric ratio (1 : 2 w/w). The mixture was incubated under gentle stirring at room temperature for 2 h to allow electrostatic interaction and adsorption of fucoidan onto the nanoparticle surface.

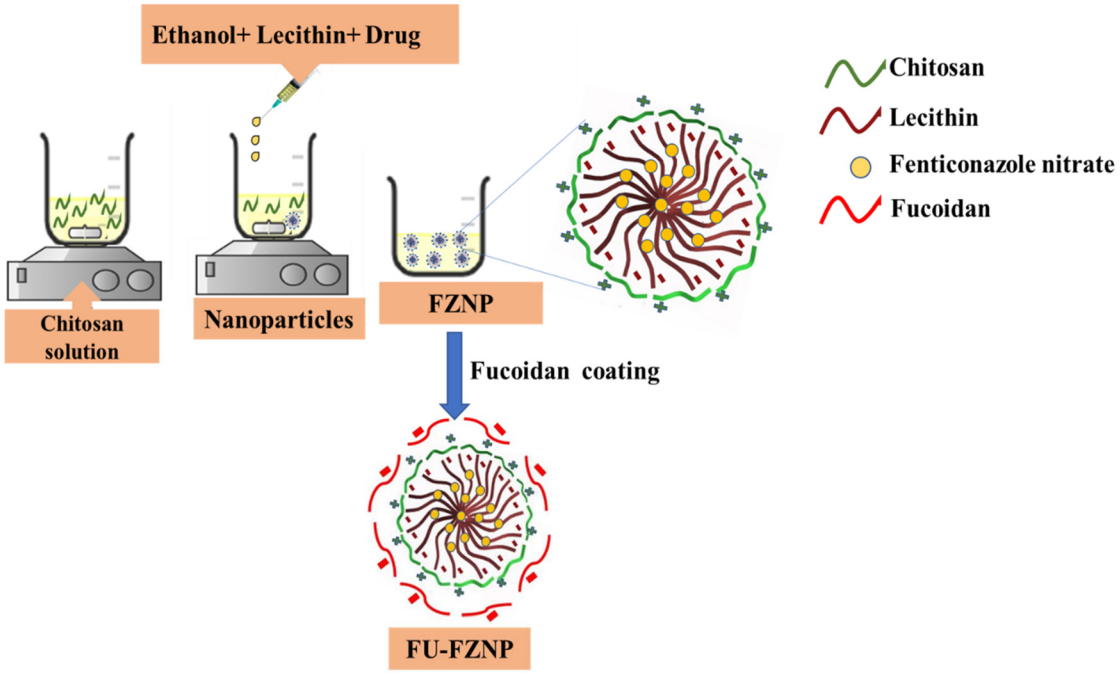

Fig. 1 Schematic representation of the formation of fenticonazole nitrate-loaded, fucoidan-coated lecithin–chitosan nanoparticles by the ethanol injection method.

Table 1 Optimization of the pharmaceutical composition of lecithin–chitosan nanoparticles

Batches	Lecithin (mg)	Chitosan (mg)	Fucoidan (mg mL^{-1})	Stirring speed (rpm)	FZN (mg)	Size (nm)	PDI	Zeta potential (mV)
FZNP-1	37.5	3	0	400	10	140.7	0.22	+37.57
FZNP-2	50	3	0	300	5	125.3	0.24	+34.78
FZNP-3	50	2.25	0	400	10	202.3	0.28	+37.12
FZNP-4	25	3	0	400	5	129.2	0.20	+34.78
FZNP-5	50	1.5	0	200	10	169.7	0.27	+37.03
FZNP-6	25	2.25	0	200	5	117.5	0.20	+36.67
FZNP-7	25	1.5	0	300	10	135.8	0.24	+31.42
FZNP-8	37.5	2.25	0	300	7.5	146.0	0.26	+25.70
FZNP-9	50	3	0	200	7.5	156.3	0.25	+41.19
FZNP-10	50	1.5	0	400	5	215.5	0.22	+10.35
FZNP-11	25	3	0	200	10	179.3	0.23	+41.27
FZNP-12	25	1.5	0	400	7.5	221.4	0.38	+45.10
FZNP-13	25	1.5	0	500	5	186.2	0.23	+45.46
FZNP-14	50	1.5	0	500	10	230.4	0.34	+61.88
FZNP-15	50	3	0	300	5	264.2	0.37	+56.19
FZNP-16	25	1.5	0	300	5	297.3	0.28	+41.98
FZNP-17	50	1.5	0	300	10	271.8	0.33	+55.14
FZNP-18	25	3	0	500	10	178.7	0.20	+58.73
FZNP-19	50	3	0	500	5	325.9	0.38	+53.22
Fu-FZNP-1	25	1.5	1.5	500	5	288.2	0.28	−38.20
Fu-FZNP-2	50	1.5	1	500	10	302.0	0.30	−49.91
Fu-FZNP-3	50	3	1	300	5	387.8	0.36	−37.61
Fu-FZNP-4	25	1.5	1	300	5	313.3	0.30	−37.79
Fu-FZNP-5	50	1.5	1.5	300	10	299.8	0.34	−46.07
Fu-FZNP-6	25	3	1	500	10	210.0	0.21	−21.32
Fu-FZNP-7	25	3	1.5	300	10	254.4	0.27	−45.19
Fu-FZNP-8	50	3	1.5	500	5	331.4	0.34	−46.55
Fu-FZNP-9	37.5	3	1	400	10	216.4	0.20	−34.63
Fu-FZNP-10	25	3	0.5	400	5	220.2	0.15	−16.16
Fu-FZNP-11	50	1.5	0.5	200	10	241.9	0.23	−19.18
Fu-FZNP-12	25	2.25	1	200	5	227.1	0.26	−26.75
Fu-FZNP-13	25	1.5	1	300	10	197.8	0.22	−36.65
Fu-FZNP-14	37.5	2.25	0.5	300	7.5	238.7	0.43	−19.11
Fu-FZNP-15	50	3	1	200	7.5	191.0	0.15	−40.89
Fu-FZNP-16	50	1.5	1	400	5	260.6	0.22	−29.75

Fucoidan and chitosan are multifunctional polymers that are capable of being ionized in an aqueous medium. Fucoidan can be expressed as FU–COOH–SO_3H/FU–COO^-–SO_3^-, and chitosan as CHI–NH_3^+/CHI–NH_2 in their protonated and deprotonated forms, respectively. The ionic cross-linking relies on favorable chitosan and fucoidan electrostatic contact, and the quantity of ionizable locations on the surface of the polymers will determine the outcome. Table 1 illustrates how fucoidan was added to the previously optimized batch. The particle size and zeta potential of the resultant nanoparticles were further examined. Rhodamine B was incorporated into the nanoparticles for *ex vivo* permeation studies by replacing fenticonazole nitrate with rhodamine B during the nanoparticle preparation process, following the same formulation protocol. The dye was dissolved in the aqueous phase prior to nanoparticle formation, allowing its entrapment within the nanoparticulate matrix. The nanoparticles were freeze-dried for further analysis.

2.2.3. Physicochemical characterization of lecithin–chitosan nanoparticles

2.2.3.1. Particle size, PDI and zeta potential. The particle size, PDI and zeta potential of FZNP and Fu-FZNP were examined with a Zetasizer (NanoZS Malvern, UK). The polystyrene cuvettes were filled with nanoparticle solutions and analyzed at 173° scattering angle at 25 ± 0.5 °C. All the samples were examined in triplicate, and the results are reported as mean ± SD (n = 3).[44,45]

2.2.3.2. ATR-FTIR analysis of nanoparticles. Chitosan (CH), fucoidan (Fu), FZN, PM (a physical mixture of lecithin, chitosan, fucoidan, drug in a 1 : 1 : 1 ratio), freeze-dried blank chitosan lecithin nanoparticles (BNP), FZNP and Fu-FZNP were examined spectroscopically using ATR-FTIR (Spectrum RX-1, PerkinElmer, US). Separately, 5 mg of freeze-dried samples were placed on the holder and scanned at a resolution of 4 cm^{-1}, covering a wavenumber spectrum of 400–4000 cm^{-1}.[46,47]

2.2.3.3. Differential scanning calorimetry (DSC) analysis of nanoparticles. DSC was used to measure the thermodynamic events of excipients and drug (STARe system, Metler Toledo, Switzerland). After weighing the samples (chitosan, fucoidan, FZN, PM, BNP, FZNP and Fu-FZNP), they were positioned in an aluminium pan and heated to an elevated temperature, in compliance with the protocol, while flowing 50 mL min^{-1} of liquid nitrogen through it. The samples were analysed over a temperature range of 25 °C to 300 °C for 10 minutes.[48]

2.2.3.4. P-XRD analysis of nanoparticles. PXRD (Empyrean, Malvern Panalytical, Worcestershire, United Kingdom) analyses of chitosan, fucoidan, FZN, PM, BNP, FZNP and Fu-FZNP were performed. The freeze-dried samples were examined at a speed of 0.0436°/sec and at 2θ angles ranging from 2 to 40°.[49,50]

2.2.3.5. Surface morphology by transmission electron microscopy (TEM). The morphology and structure of FZNP and Fu-FZNP were evaluated by TEM (JEM1400 TEM; JEOL, Tokyo, Japan) with 500 k magnification and 120 kV illumination (installed at the National Institute of Animal Biology (NIAB), Hyderabad). The nanoparticles were allowed to dry on a small carbon-coated grid and viewed with the microscope at a suitable magnification. The samples were prepared on a carbon grid and negatively stained with a 1% uranyl acetate. Microphotographs of FZNP and Fu-FZNP were recorded at appropriate magnification.[51]

2.2.4. Drug loading and entrapment efficiency. The entrapment efficiency and drug loading of FZNP and Fu-FZNP were estimated by an indirect technique with the aid of RP-HPLC at 252 nm wavelength. The FZNP and Fu-FZNP were centrifuged (Micro ultracentrifuge, Sorval Mx150+, Thermo Fisher Scientific, US) at 50 000 ± 100 rpm for 2 h at 4 ± 0.5 °C. Following centrifugation, the clear supernatant containing the unentrapped drug was carefully collected without disturbing the nanoparticle pellet. To ensure complete removal of surface-associated drug, the nanoparticle pellet was washed twice with buffer, followed by centrifugation under the same conditions. The wash supernatants were pooled with the initial supernatant. The supernatant was collected, diluted with methanol, and further analyzed by RP-HPLC, based on a previously constructed calibration curve. The % entrapment efficiency and drug loading were estimated using eqn (1) and (2), respectively.

$$\%\,\text{Entrapment efficiency} = \frac{\text{Drug entrapped in pellet}}{\text{Amount of drug added}} \times 100 \quad (1)$$

$$\%\,\text{Drug loading} = \frac{\text{Entrapped drug amount}}{\text{Amount of lipid used}} \times 100 \quad (2)$$

2.2.5. *In vitro* interaction of mucin with FZNP and Fu-FZNP. To study the *in vitro* interaction of mucin with the developed nanoparticles, gastric mucin was used. A 1 mL mucin solution (2 mg mL^{-1}) was combined with 1 mL of FZNP and Fu-FZNP, and the mixture was constantly agitated for 1 h at 37 ± 0.5 °C.[52] The particle size and zeta potential of the nanoparticles were measured using the Zetasizer. All measurements were performed in triplicate and recorded as an average with standard deviation.

2.2.6. *Ex vivo* permeation studies. Fresh goat vaginal mucosa was obtained from a local abattoir from healthy adult animals of approximately [6–12 months] immediately after slaughter. The excised tissue was washed with cold normal saline to remove adhering blood and debris and transported to the laboratory in ice-cold phosphate-buffered saline (PBS, pH 7.4) within 1–2 h of collection. Upon arrival, excess connective tissue and fat were carefully removed, and the mucosal layer was separated using blunt dissection. The tissue was stored at 4 °C in PBS and used within 24 h to preserve viability. Fresh goat vaginal mucosa procured from the slaughterhouse was placed below the donor compartment and above the receptor compartments of a locally constructed Franz's diffusion cell, which had a diffusion area of 4.9 cm^2, to test *ex vivo* permeation. The FZNP and Fu-FZNP samples were positioned into the cell donor. The receptor compartment was kept at 37 ± 0.5 °C and contained 25 mL of simulated vaginal fluid (pH 4.5) with 25% methanol to create a sink condition. Parafilm was used to properly seal the system. An equivalent volume of

fresh permeation medium was added to replace the 0.5 mL sample withdrawn. The collected samples were passed through a 0.45 μm membrane filter and analyzed by a validated HPLC method at a wavelength of 252 nm. The permeation flux (J_{max}) was assessed using eqn (3):[53]

$$J_{max} = \frac{\text{Amount of FZN Permeated}}{\text{Time} \times \text{Area of membrane}} \quad (3)$$

2.2.7. *In vitro* antimicrobial activity. The *Staphylococcus aureus* (*S. Aureus*) (ATCC 29213) and *Candida albicans* (*C. albicans*) (MTCC 183), Gram-positive bacterial and fungal strains, were used to estimate the antimicrobial activity of FZN, FZNP and Fu-FZNP. The stock cultures were kept at 4 °C on Sabouraud dextrose agar medium for fungi and Muller-Hinton agar for bacteria. The antibacterial activity was investigated using the agar-well diffusion method. The tests were run on Sabouraud dextrose agar for fungus and Muller-Hinton agar for bacteria. The samples were placed on the plates and incubated for 24 h at 30 °C for bacteria and 48 h at 37 °C for fungi. A zone of inhibition representing the antibacterial and antifungal activity was identified. Photos and measurements of the diameter of the inhibition zones were taken.

2.2.8. Stability study of FZNP and Fu-FZNP. The stability studies of the samples were performed at 5 ± 3 °C and 25 ± 3 °C for 1 month. The samples were tested for physical appearance, particle size, PDI, zeta potential and entrapment efficiency. All the samples were analyzed in triplicate and reported as the mean ± SD.

2.2.9. Statistical analysis. The experimental data are presented as the mean ± standard deviation (SD). Statistical analysis was performed using analysis of variance (ANOVA) or Tukey's multiple comparison test in GraphPad Prism version 8.0 (GraphPad Software Inc., CA, USA). A *p*-value of less than 0.05 was considered statistically significant.

3. Results and discussion

3.1. Optimization of FZNP and Fu-FZNP

A total of 36 batches were designed, developed, and characterized by varying the process and excipient-related attributes. The batches were optimized based on physical appearance, particle size, PDI and zeta potential, as shown in Table 1. In the current work, ethanolic lecithin/FZN solution was injected into an aqueous chitosan solution to produce lecithin–chitosan nanoparticles. As illustrated in Fig. 1, positively charged chitosan and negatively charged lecithin interacted through self-assembly. The resulting nanoparticles were clear and blue in appearance. As indicated in Table 1, their characteristics were determined by measuring the mean particle size, zeta potential and PDI. It is believed that the positively charged chitosan covering of the nanoparticles' surface is the cause of their higher positive zeta potential.

The material attributes utilized in the optimization of the formulation were the concentrations of drug, lecithin, chitosan, and fucoidan, followed by process parameters, including stirring speed and rate of addition. The amount of lecithin, chitosan and fucoidan had positive effects on the size and PDI. The stirring speed and the rate of addition had negative effects on the size. The concentration of lecithin was fixed at 25 mg, and chitosan at 3 mg, and the amount of drug was varied from 5 mg to 10 mg as the optimized batch, with a stirring speed of 500 rpm. The zeta potential increased with an increase in the chitosan amount and decreased with an increase in the lecithin amount. The fucoidan addition for altering the zeta potential resulted in increased particle size and a negative potential for Fu-FZNP. The optimized batch was further characterized and evaluated.

3.2. Physicochemical characterization of nanoparticles

3.2.1. Particle size, PDI and zeta potential of nanoparticles. The dynamic light scattering method was utilized to analyze the particle size and PDI. The particle sizes of the optimized formulations of FZNP and Fu-FZNP were found to be 129.20 ± 0.25 nm and 227.10 ± 1.54 nm, and the PDI was found to be 0.21 ± 0.003 and 0.26 ± 0.01, respectively, as shown in Fig. 2IC and IIC. The zeta potential of FZNP and Fu-FZNP were found to be +30.96 ± 1.15 mV and −26.75 ± 0.3 mV, respectively, as shown in Fig. 2ID and IID. The particle size of the nanoparticles increased upon coating with fucoidan, and the zeta potential changed from positive in FZNP to negative in Fu-FZNP, indicating the formation of modified nanoparticles.

3.2.2. Surface morphology of FZNP and Fu-FZNP. The surface morphologies of the formulated FZNP and Fu-FZNP are illustrated in Fig. 2IB and IIB. The nanoparticles exhibited a spherical appearance with a smooth surface and were uniformly dispersed with no drug precipitation, which indicated the stability of the fabricated system.

3.2.3. ATR-FTIR analysis of the nanoparticles. ATR-FTIR analysis was carried out to investigate the compatibility of the drug with excipients and drug encapsulation in the nanoparticles. The spectra of CH, Fu, Le, PM, BNP, FZNP, and Fu-FZNP are compiled and displayed in Fig. 3. The characteristic peaks corresponding to the C═N of the imidazole group (1578 cm^{-1}), C–H (1465 cm^{-1}), ν(C═C) (1403 cm^{-1}), C–N (1295 cm^{-1}), C–O–C (1118 cm^{-1}), C–S (733 cm^{-1}), and C–Cl (626 cm^{-1}) were identified for FZN. The CH spectra exhibited peaks for C═N (1577 cm^{-1}), C═O (1653 cm^{-1}), C–O–C (1176 cm^{-1}), and C–O (1054 cm^{-1}). Fu exhibited peaks for S═O (1165–1220 cm^{-1}), and C–O–S (812 cm^{-1}), and the C–H (2922 cm^{-1} and 2853 cm^{-1}) stretching band of the long fatty acid chain was observed for lecithin. PM illustrated all the characteristic peaks pertaining to the drug and excipients, without the formation of any new bonds, indicating the absence of interaction between the drug and excipients. The FZNP and Fu-FZNP exhibited characteristic peaks of CH, Fu, and Le with a redshift of the peak positions. The characteristic peaks of the drug were not observed in FZNP and Fu-FZNP, indicating the encapsulation of FZN in the nanoparticles.

3.2.4. DSC analysis of nanoparticles. Thermal events for CH, Fu, PM, BNP, FZNP, and Fu-FZNP were observed using

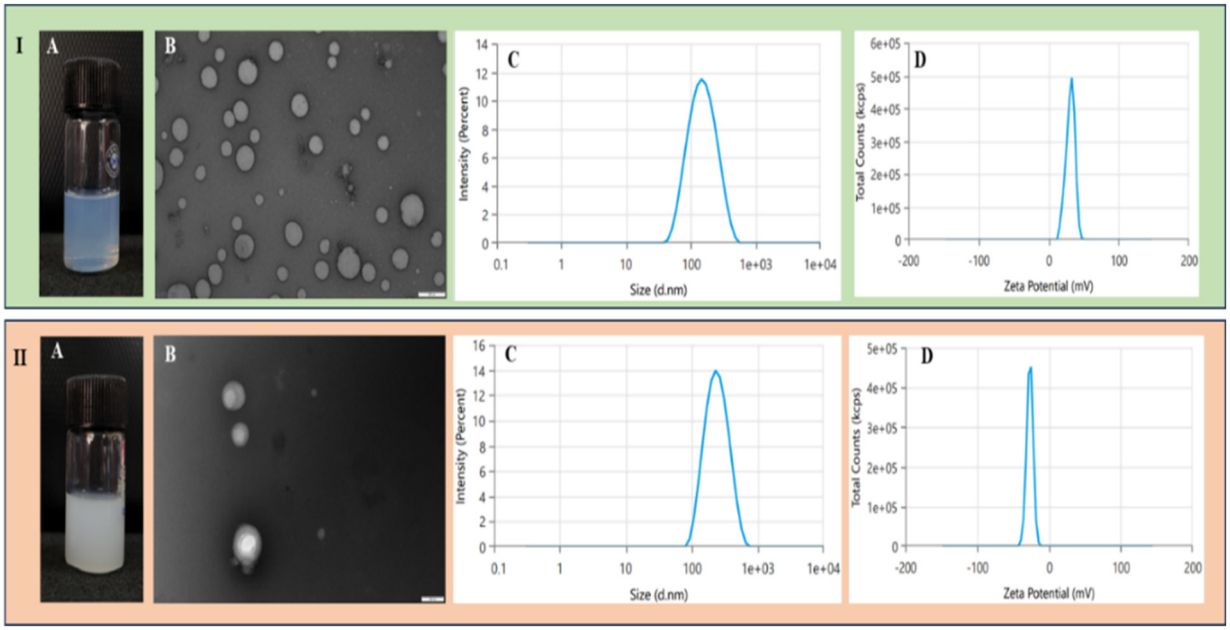

Fig. 2 Lecithin–chitosan nanoparticles: (A) morphology of FZNP, (B) TEM microscopic image of FZNP at a scale of 500 nm, (C) particle size of FZNP, and (D) zeta potential of FZNP. (II) Fucoidan-coated lecithin–chitosan nanoparticles: (A) morphology of Fu-FZNP, (B) TEM microscopic image of Fu-FZNP at a scale of 200 nm, (C) particle size of Fu-FZNP, and (D) zeta potential of Fu-FZNP.

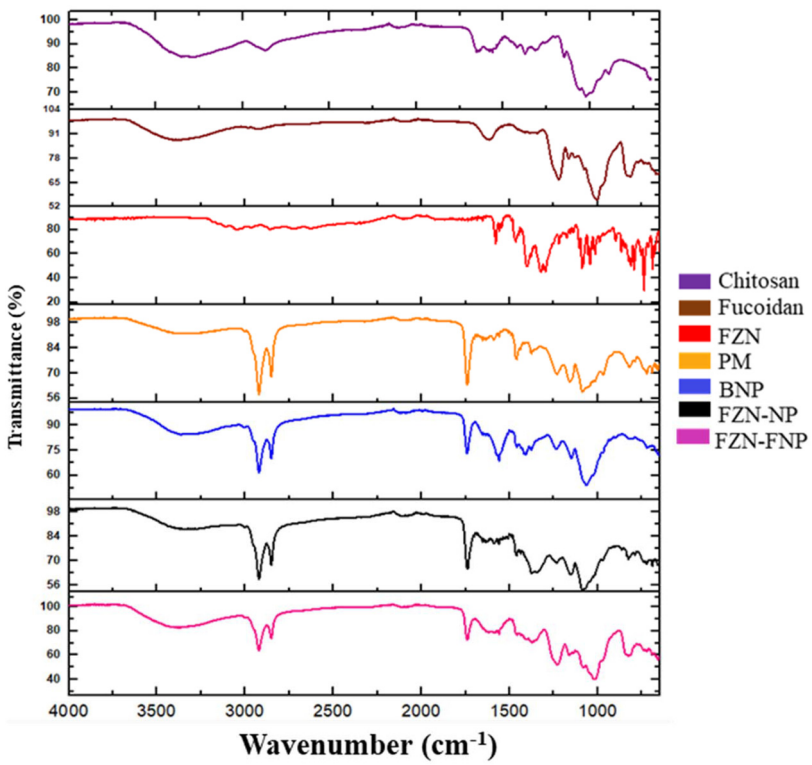

Fig. 3 FTIR spectra of chitosan, fucoidan, FZN, PM, BNP, FZNP and Fu-FZNP.

DSC, as illustrated in Fig. 4. The DSC thermogram of FZN exhibits an endothermic peak at 140 °C, corresponding to the melting point of the crystalline FZN. On the other hand, the FZNP curve did not show the melting peak of the crystalline FZN, suggesting that the FZN has been uniformly dispersed in the polymer and lipid matrix. Similarly, the FZN melting peak

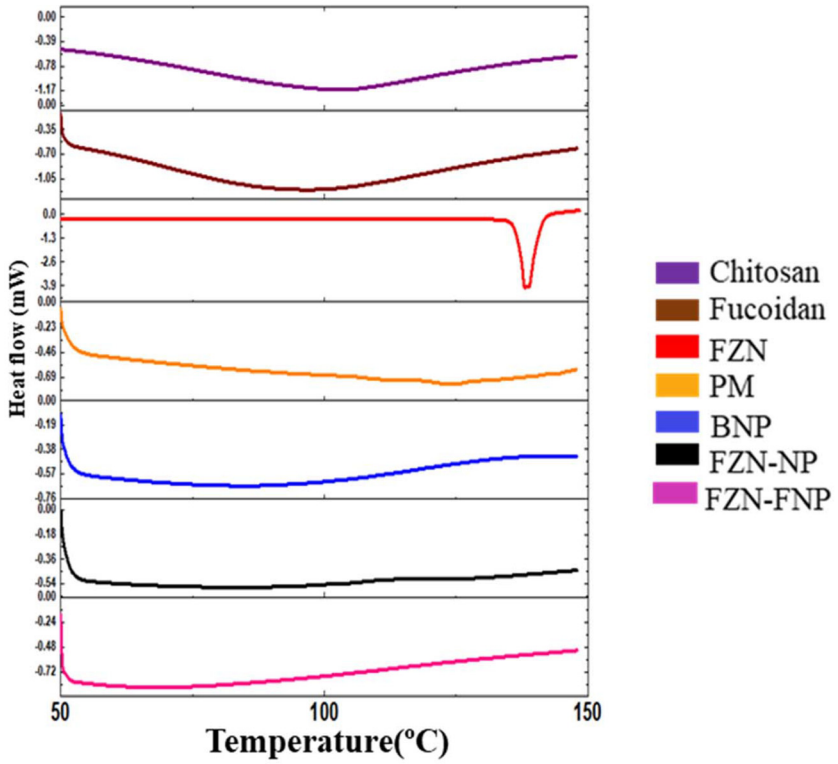

Fig. 4 DSC thermograms of chitosan, fucoidan, FZN, PM, BNP, FZNP and Fu-FZNP.

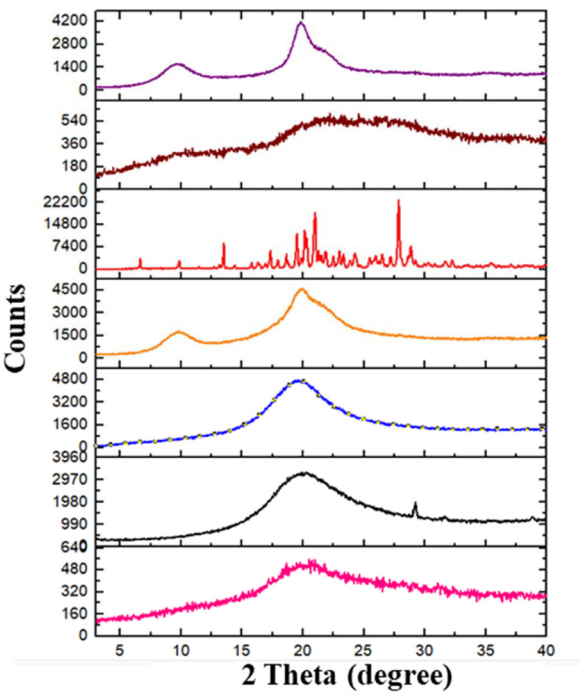

Fig. 5 XRD patterns of chitosan, fucoidan, FZN, PM, BNP, FZNP and Fu-FZNP.

was absent in the Fu-FZNP DSC curve, indicating that FZN dispersibility in FZNP persisted in the coated nanoparticles.

3.2.5. P-XRD analysis of nanoparticles. XRD analysis of the samples was performed to estimate the form of FZN in FZNP and Fu-FZNP. The diffractograms of CH, Fu, PM, BNP, FZNP, and Fu-FZNP are illustrated in Fig. 5. The distinctive peaks of FZN were not found in FZNP and Fu-FZNP. The peaks of the formulation and the polymer aligned, indicating that the FZN was fully dispersed within the high concentrations of lipid–polymer and was enclosed in the nanoparticulate matrix. The diffractogram of the Fu-FZNP was in line with that of the Fu, indicating the coating of the FZNP. These outcomes confirmed that FZN had been effectively encapsulated in FZNP and Fu-FZNP.

3.2.6. Entrapment efficiency. The FZNP and Fu-FZNP showed % EE of 65.47% ± 2.32% and 71.13% ± 5.74%. The % drug loadings of FZNP and Fu-FZNP were 11.69% ± 0.41% and 7.41% ± 0.60%, respectively. The % entrapment efficiency of the fucoidan-coated batch was approximately 7% more compared to that of the uncoated nanoparticles. The drug loading capacity of the uncoated nanoparticles was higher when compared to that of the coated nanoparticles because the modified particles included the weight of the fucoidan coating polymer, which, in turn, increased the net weight of the nanoparticle.

3.2.7. *In vitro* interaction of mucin with FZNP and Fu-FZNP. Mucus is a linear peptide chain consisting of 8–169 amino acids that has repeating proline, threonine, and serine domains. It is hydrophilic and highly negatively charged. The

mucus prevents interactions between particles, and it is highly effective at removing nanoparticles through a variety of adhesive interactions, including hydrogen bonding, hydrophobic interactions, and electrostatic interaction potentials. The zeta potential and particle size of nanoparticles following co-incubation with mucin at 37 °C are displayed in Fig. 6IA and IB. It was observed that, following a one-hour incubation period with mucus, the mean particle size of FZNP grew dramatically. This suggests that the particle was able to interface with the negatively charged mucin with ease and form a large complex because of strong electrostatic attraction. Nevertheless, the improvement of Fu-FZNP modification did not significantly increase the particle sizes, suggesting only a slight interaction with the negatively charged mucin. Hence, it can be assumed that the zeta potential modified nanoparticles, Fu-FZNP, did not interact with the negatively charged mucin.

3.2.8. *Ex vivo* permeation studies. To assess the impact of fucoidan-coated lecithin–chitosan nanoparticles on the permeability across the stratum corneum, skin permeation parameters were measured using FZNP and Fu-FZNP. The flux of the nanoparticles to transport the drug around the vaginal mucus of the goat and the stratum corneum was followed by plotting a graph of the percentage cumulative amount of drug absorbed across a unit area of skin with respective time (Fig. 6IC). The *ex vivo* permeation studies through the skin exhibited 61.74% ± 2.07% and 72.11% ± 1.4% of FZN from FZNP and Fu-FZNP, respectively, as shown in Fig. 6IC. The FZNP showed a flux of 151.21 μg cm^{-2} h^{-1}, and Fu-FZNP showed a flux of 176.58 μg cm^{-2} h^{-1}. Fig. 6II illustrates how

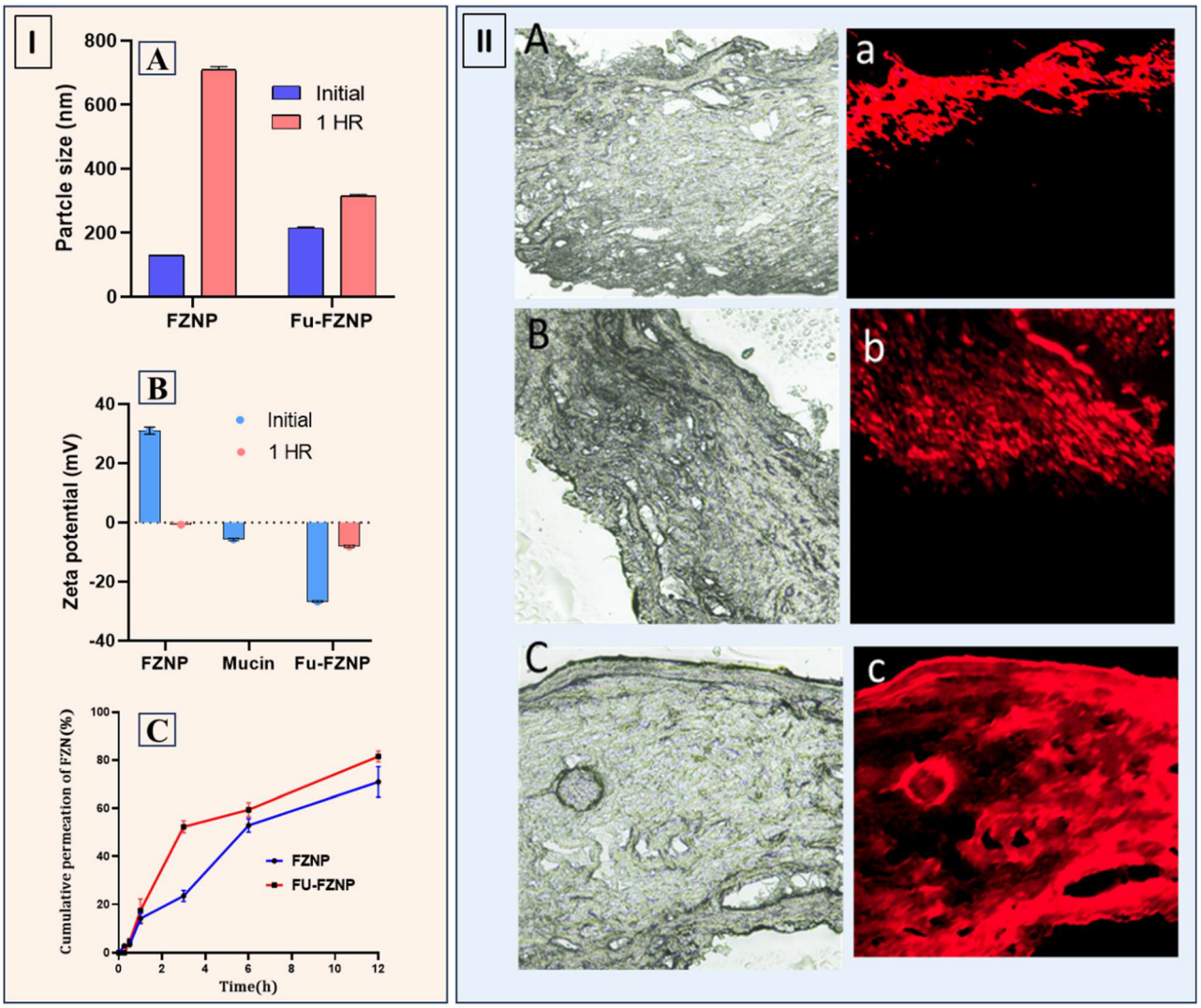

Fig. 6 (I) (A) Particle size after interaction of mucin with FZNP and Fu-FZNP. (B) Zeta potential interaction of mucin with FZNP and Fu-FZNP (C) *ex vivo* permeation graph of FZNP and Fu-FZNP. The data are represented as mean ± SD (n = 3). (II) Normal light microscopic images of goat vagina after the application of (A) rhodamine B solution, (B) rhodamine B-labeled FZN-NP, and (C) rhodamine B-labeled Fu-FZNP after 12 h. Fluorescence images of (a) rhodamine B solution, (b) rhodamine B-labeled FZN-NP, and (c) rhodamine B labeled Fu-FZNP after 12 h.

Table 2 Stability studies on FZNP and Fu-FZNP

Batch	Sample interval	Stability conditions	Physical appearance	Particle size (nm)	PDI	Zeta potential	Entrapment efficiency (%)
FZNP	Initial	—	Bluish transparent	129.20 ± 0.25	0.21 ± 0.003	30.96 ± 1.15	65.46 ± 2.32
	1 month	5 ± 3 °C		130.20 ± 0.62	0.20 ± 0.004	32.74 ± 1.70	62.01 ± 1.63
		25 ± 3 °C		135.15 ± 0.73	0.24 ± 0.01	34.35 ± 1.06	61.97 ± 1.92
Fu-FZNP	Initial	—	Milky white	227.10 ± 0.26	0.26 ± 0.01	26.75 ± 0.32	73.14 ± 1.23
	1 month	5 ± 3 °C		228.83 ± 0.85	0.27 ± 0.008	29.89 ± 0.38	70.09 ± 2.39
		25 ± 3 °C		224.13 ± 0.82	0.30 ± 0.036	26.92 ± 0.606	68.42 ± 2.64

intimate contact with superficial junctions may have allowed the superficial dispersion of active substances, leading to a possible modest penetration of rhodamine B solution. The findings concluded that rhodamine B labeled FZN-NP and Fu-FZNP penetrate deep layers of the excised goat vagina.

3.2.9. Stability study of FZNP and Fu-FZNP. The stability studies data of FZNP and Fu-FZNP are listed in Table 2. The stability parameter did not show any significant change in physical appearance, particle size, PDI, zeta potential or entrapment efficiency. Stability testing over longer durations (*e.g.*, three months or more) in physiologically relevant media would provide a more comprehensive understanding of formulation performance and storage behavior. These aspects are planned to be addressed in future studies.

3.2.10. *In vitro* antimicrobial activity. The results of qualitative antimicrobial activity assessment of FZN, FZNP and Fu-FZNP by the agar-well diffusion method are reported in Fig. 7I and II. The zone of inhibition values of FZNP and Fu-FZNP were 13.17 ± 0.62 mm and 11.33 ± 0.85 mm, respectively, for *Staphylococcus aureus*. The zone of inhibition values of FZNP and Fu-FZNP were 19.83 ± 0.94 mm and 21.67 ± 0.47 mm, respectively, for *Candida albicans*. Increases in the concentration caused increases in the zone of inhibition. The developed formulations exhibited both antibacterial and antifungal activity, providing evidence of their suitability to treat mixed vaginal infections. In the present study, antimicrobial activity was assessed using the agar-well diffusion assay, which serves as a qualitative screening method to indicate inhibitory effects of the developed formulation. As the principal aim of this work was formulation optimization and preliminary biological evaluation, quantitative antimicrobial susceptibility tests such as minimum inhibitory concentration (MIC) determination and time–kill kinetics were not conducted. It is recognized that MIC and time–kill assays provide more precise and comprehensive measures of antimicrobial efficacy and kinetics than agar diffusion methods, and the lack of these assays represents a limitation of the current study. Future work will incorporate standardized MIC and time–kill analyses to quantitatively evaluate the antimicrobial activity of the formulation and to substantiate its potential

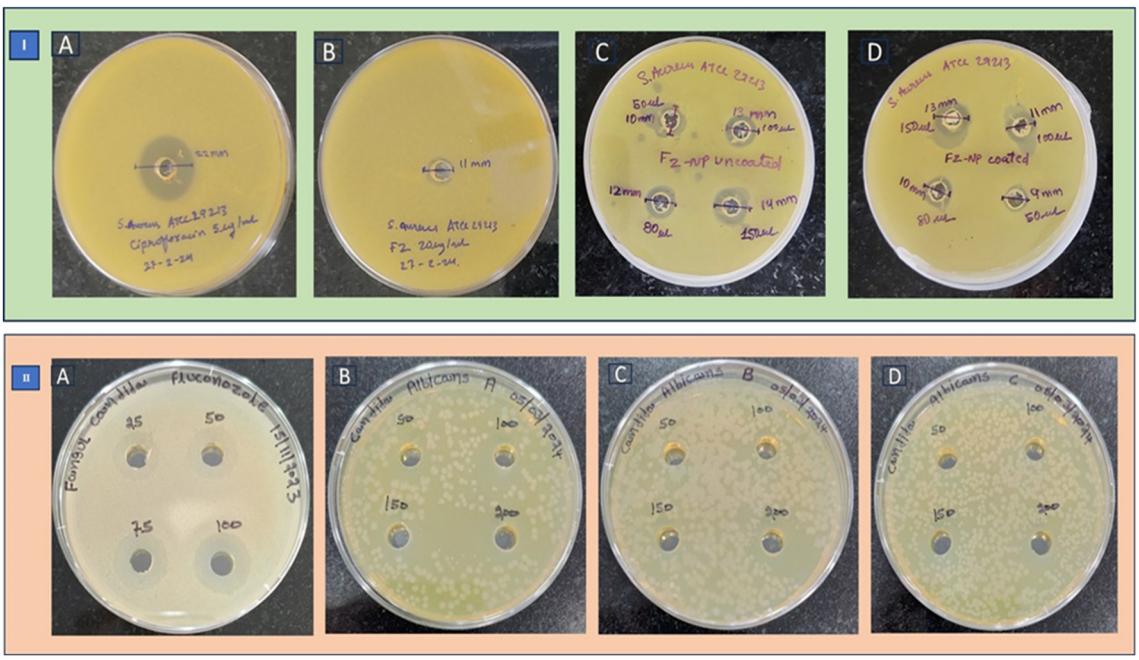

Fig. 7 (I) *In vitro* antibacterial activity of patches against *Staphylococcus aureus*: (A) standard, (B) FZN, (C) FZNP, and (D) Fu-FZNP. (II) *In vitro* antifungal activity of patches against *Candida albicans*: (A) standard, (B) FZN, (C) FZNP, and (D) Fu-FZNP.

efficacy against mixed bacterial and fungal infections under defined conditions.

4. Conclusion

In the present investigation, lecithin–chitosan nanoparticles and fucoidan-coated nanoparticles loaded with FZN for the management of mixed vaginal infections were formulated and evaluated. The FZNP and Fu-FZNP were developed by using the ethanol injection technique, and the nanoparticles displayed a mean particle size of 129.20 ± 0.25 nm, a PDI of 0.21 ± 0.003 and a zeta potential of +30.96 ± 1.15 mV. Furthermore, the fucoidan-coated zeta potential modulated nanoparticles were prepared by incubating FZNP with fucoidan. The optimized zeta potential modulating nanoparticles displayed a mean particle size of 227.10 ± 1.54 nm, a PDI of 0.26 ± 0.01 and a zeta potential of −26.75 ± 0.3 mV. The physicochemical characterization proved the encapsulation of FZN in the nanoparticles and that the coating of fucoidan resulted in zeta potential modified nanoparticles that can cross the mucus barrier and prevent back diffusion. The entrapment efficiency of FZNP and Fu-FZNP was 65.47% ± 2.32% and 71.13% ± 5.74%, with 11.69% ± 0.414% (FZNP) and 7.41% ± 0.60% (Fu-FZNP) drug loading. The spherical morphologies of the nanoparticles were confirmed by TEM imaging. The amount of drug permeated through the excised goat vagina was found to be 61.74% ± 2.07% and 72.11% ± 1.4% for FZNP and Fu-FZNP, respectively. The *in vitro* antimicrobial activity of FZNP and Fu-FZNP showed antibacterial action against *Staphylococcus aureus* and antifungal activity against *Candida albicans* species. These results indicate that FZN and Fu-FZNP lecithin–chitosan nanoparticles could be further developed for safe, convenient, and effective treatment of mixed vaginal infections.

Conflicts of interest

The authors report no conflict of interest related to the manuscript.

Data availability

Data will be available upon request.

Acknowledgements

The authors would like to thank all individuals who contributed to this work. Their support and insights were invaluable to the completion of this study.

References

1 J. D. Sobel, C. Subramanian, B. Foxman, M. Fairfax and S. E. Gygax, Mixed vaginitis - More than coinfection and with therapeutic implications, *Curr. Infect. Dis. Rep.*, 2013, **15**(2), 104–108, DOI: 10.1007/S11908-013-0325-5/METRICS.
2 V. Goel, P. Bhalla, A. Sharma and Y. M. Mala, Lower genital tract infections in HIV-seropositive women in India, *Indian J. Sex. Transm. Dis. AIDS*, 2011, **32**(2), 103–107.
3 J. Bornstein and D. Zarfati, A Universal Combination Treatment for Vaginitis, *Gynecol. Obstet. Invest.*, 2008, **65**(3), 195–200, DOI: 10.1159/000111946.
4 M. Sanguinetti, E. Cantón, R. Torelli, F. Tumietto, A. Espinel-Ingroff and B. Posteraro, In vitro activity of fenticonazole against Candida and bacterial vaginitis isolates determined by mono- Or dual-species testing assays, *Antimicrob. Agents Chemother.*, 2019, **63**(7), 10–128, DOI: 10.1128/AAC.02693-18.
5 R. Albash, A. M. Al-Mahallawi, M. Hassan and A. A. Alaa-Eldin, Development and Optimization of Terpene-Enriched Vesicles (Terpesomes) for Effective Ocular Delivery of Fenticonazole Nitrate: In vitro Characterization and in vivo Assessment, *Int. J. Nanomed.*, 2021, **16**, 609–621, DOI: 10.2147/IJN.S274290.
6 S. Veraldi and R. Milani, Topical fenticonazole in dermatology and gynaecology: Current role in therapy, *Drugs*, 2008, **68**(15), 2183–2194, DOI: 10.2165/00003495-200868150-00007.
7 A. L. Costa, A. Valenti and M. Veronese, Study of the Morphofunctional Alterations Produced by Fenticonazole on Strains of Candida albicans, using the Scanning Electron Microscope (S. E. M.), *Mycoses*, 1984, **27**(1), 29–35, DOI: 10.1111/J.1439-0507.1984.TB01979.X.
8 A. Costa, M. Veronese, P. Puggeri and A. Valenti, Ultrastructural findings of Candida albicans blastoconidia submitted to the action of fenticonazole, *Arzneimittelforschung*, 1989, **39**(2), 230–233. Accessed: Jun. 24, 2025. [Online]. Available: https://europepmc.org/article/med/2659001.
9 J. Fernández-Alba, *et al.*, Fenticonazole Nitrate for Treatment of Vulvovaginitis: Efficacy, Safety, and Tolerability of 1-Gram Ovules, Administered as Ultra-Short 2-Day Regimen, *J. Chemother.*, 2004, **16**(2), 179–186, DOI: 10.1179/JOC.2004.16.2.179.
10 F. Gorlero, A. Sartani, C. I. Cordaro, D. Bertin, C. Reschiotto and L. De Cecco, Fenticonazole tissue levels after the application of 3 different dosage forms of vaginal ovules, *Int. J. Clin. Pharmacol. Ther. Toxicol.*, 1988, **26**(10), 479–481.
11 R. Albash, C. Yousry, A. M. Al-Mahallawi and A. A. Alaa-Eldin, Utilization of PEGylated cerosomes for effective topical delivery of fenticonazole nitrate: *in vitro* characterization, statistical optimization, and *in vivo* assessment, *Drug Delivery*, 2021, **28**(1), 1–9, DOI: 10.1080/10717544.2020.1859000.
12 S. Veraldi and R. Milani, Topical fenticonazole in dermatology and gynaecology: Current role in therapy, *Drugs*, 2008, **68**(15), 2183–2194, DOI: 10.2165/00003495-200868150-00007.
13 S. Srikrishna and L. Cardozo, The vagina as a route for drug delivery: A review, *Int. Urogynecol. J. Pelvic. Floor*

Dysfunct., 2013, **24**(4), 537–543, DOI: 10.1007/S00192-012-2009-3.

14 C. M. Caramella, S. Rossi, F. Ferrari, M. C. Bonferoni and G. Sandri, Mucoadhesive and thermogelling systems for vaginal drug delivery, *Adv. Drug Delivery Rev.*, 2015, **92**, 39–52, DOI: 10.1016/j.addr.2015.02.001.

15 R. Palmeira-de-Oliveira, A. Palmeira-de-Oliveira and J. Martinez-de-Oliveira, New strategies for local treatment of vaginal infections, *Adv. Drug Delivery Rev.*, 2015, **92**, 105–122, DOI: 10.1016/j.addr.2015.06.008.

16 J. das Neves, R. Nunes, A. Machado and B. Sarmento, Polymer-based nanocarriers for vaginal drug delivery, *Adv. Drug Delivery Rev.*, 2015, **92**, 53–70, DOI: 10.1016/j.addr.2014.12.004.

17 G. Chindamo, S. Sapino, E. Peira, D. Chirio and M. Gallarate, Recent advances in nanosystems and strategies for vaginal delivery of antimicrobials, *Nanomaterials*, 2021, **11**(2), 1–29, DOI: 10.3390/NANO11020311.

18 B. Valamla, *et al.*, Engineering drug delivery systems to overcome the vaginal mucosal barrier: Current understanding and research agenda of mucoadhesive formulations of vaginal delivery, *J. Drug Delivery Sci. Technol*, 2022, **70**, 103162, DOI: 10.1016/J.JDDST.2022.103162.

19 J. das Neves, M. Amiji and B. Sarmento, Mucoadhesive nanosystems for vaginal microbicide development: Friend or foe?, *Wiley Interdiscip. Rev.: Nanomed. Nanobiotechnol.*, 2011, **3**(4), 389–399, DOI: 10.1002/WNAN.144.

20 R. Bansil and B. S. Turner, Mucin structure, aggregation, physiological functions and biomedical applications, *Curr. Opin. Colloid Interface Sci.*, 2006, **11**(2–3), 164–170, DOI: 10.1016/J.COCIS.2005.11.001.

21 K. Netsomboon and A. Bernkop-Schnürch, Mucoadhesive vs. mucopenetrating particulate drug delivery, *Eur. J. Pharm. Biopharm.*, 2016, **98**, 76–89, DOI: 10.1016/J.EJPB.2015.11.003.

22 B. Le-Vinh, N. M. N. Le, I. Nazir, B. Matuszczak and A. Bernkop-Schnürch, Chitosan based micelle with zeta potential changing property for effective mucosal drug delivery, *Int. J. Biol. Macromol.*, 2019, **133**, 647–655, DOI: 10.1016/J.IJBIOMAC.2019.04.081.

23 L. M. Hemmingsen, N. Škalko-Basnet and M. W. Jøraholmen, The expanded role of chitosan in localized antimicrobial therapy, *Mar. Drugs*, 2021, **19**(12), 697, DOI: 10.3390/MD19120697.

24 K. A. Janes, P. Calvo and M. J. Alonso, Polysaccharide colloidal particles as delivery systems for macromolecules, *Adv. Drug Delivery Rev.*, 2001, **47**(1), 83–97, DOI: 10.1016/S0169-409X(00)00123-X.

25 S. A. Agnihotri, N. N. Mallikarjuna and T. M. Aminabhavi, Recent advances on chitosan-based micro- and nanoparticles in drug delivery, *J. Controlled Release*, 2004, **100**(1), 5–28, DOI: 10.1016/J.JCONREL.2004.08.010.

26 Stabilization of colloidal systems by the formation of ionic lipid-polysaccharide complexes, May 1996.

27 S. Batzri and E. D. Korn, Single bilayer liposomes prepared without sonication, *Biochim. Biophys. Acta, Biomembr.*, 1973, **298**(4), 1015–1019, DOI: 10.1016/0005-2736(73)90408-2.

28 Liposome Drug Delivery Systems - Guru V. Betageri, Scott Allen Jenkins, Daniel Parsons - Google Books. Accessed: Jun. 27, 2025. [Online]. Available: https://books.google.co.in/books?hl=en&lr=&id=RI8sEQAAQBAJ&oi=fnd&pg=PP1&dq=G.+V.+Betageri,+S.+A.+Jenkins,+and+D.+L.+Parsons,+Liposome+drug+delivery+systems.+Technomic+Pub,+1993.+Accessed:+Mar.+07,+2024.+&per;5BOnline&per;5D.+Available:+https://www.routledge.com/Liposome-Drug-Delivery-Systems/Betageri-Jenkins-Parsons/p/book/9781566760300&ots=0pe8hiVm4f&sig=XJJljDOyh35YwuaoqGbRGIbumNE&redir_esc=y&hash;v=onepage&q&f=false.

29 H. Takeuchi, Y. Matsui, H. Yamamoto and Y. Kawashima, Mucoadhesive properties of carbopol or chitosan-coated liposomes and their effectiveness in the oral administration of calcitonin to rats, *J. Controlled Release*, 2003, **86**(2–3), 235–242, DOI: 10.1016/S0168-3659(02)00411-X.

30 I. Henriksen, S. R. Vågen, S. A. Sande, G. Smistad and J. Karlsen, Interactions between liposomes and chitosan II: Effect of selected parameters on aggregation and leakage, *Int. J. Pharm.*, 1997, **146**(2), 193–203, DOI: 10.1016/S0378-5173(96)04801-6.

31 I. Henriksen, G. Smistad and J. Karlsen, Interactions between liposomes and chitosan, *Int. J. Pharm.*, 1994, **101**(3), 227–236, DOI: 10.1016/0378-5173(94)90218-6.

32 E. A. Ho, V. Vassileva, C. Allen and M. Piquette-Miller, In vitro and in vivo characterization of a novel biocompatible polymer–lipid implant system for the sustained delivery of paclitaxel, *J. Controlled Release*, 2005, **104**(1), 181–191, DOI: 10.1016/J.JCONREL.2005.02.008.

33 J. Grant, M. Blicker, M. Piquette-Miller and C. Allen, Hybrid films from blends of chitosan and egg phosphatidylcholine for localized delivery of paclitaxel, *J. Pharm. Sci.*, 2005, **94**(7), 1512–1527, DOI: 10.1002/JPS.20379.

34 F. Sonvico, *et al.*, Formation of self-organized nanoparticles by lecithin/chitosan ionic interaction, *Int. J. Pharm.*, 2006, **324**(1), 67–73, DOI: 10.1016/J.IJPHARM.2006.06.036.

35 I. A. Walbi, *et al.*, Development of a Curcumin-Loaded Lecithin/Chitosan Nanoparticle Utilizing a Box-Behnken Design of Experiment: Formulation Design and Influence of Process Parameters, *Polymers*, 2022, **14**(18), 3758, DOI: 10.3390/POLYM14183758.

36 L. M. Hemmingsen, V. Panzacchi, L. M. Kangu, B. Giordani, B. Luppi and N. Škalko-Basnet, Lecithin and Chitosan as Building Blocks in Anti-Candida Clotrimazole Nanoparticles, *Pharmaceuticals*, 2023, **16**(6), 790, DOI: 10.3390/PH16060790.

37 A. Hafner, J. Lovrić, D. Voinovich and J. Filipović-Grčić, Melatonin-loaded lecithin/chitosan nanoparticles: Physicochemical characterisation and permeability through Caco-2 cell monolayers, *Int. J. Pharm.*, 2009, **381**(2), 205–213, DOI: 10.1016/J.IJPHARM.2009.07.001.

38 Q. Tan, W. Liu, C. Guo and G. Zhai, Preparation and evaluation of quercetin-loaded lecithin-chitosan nanoparticles for topical delivery, *Int. J. Nanomed*, 2011, **10**, 1621–1630.

39 I. Özcan, E. Azizoğlu, T. Senyiğit, M. Özyazici and Ö. Özer, Enhanced dermal delivery of diflucortolone valerate using

lecithin/chitosan nanoparticles: *in vitro* and *in vivo* evaluations, *Int. J. Nanomed.*, 2013, **8**, 461–475, DOI: 10.2147/IJN.S40519.

40 M. Saha, *et al.*, QbD based development of resveratrol-loaded mucoadhesive lecithin/chitosan nanoparticles for prolonged ocular drug delivery, *J. Drug Delivery Sci. Technol.*, 2021, **63**, 102480, DOI: 10.1016/J.JDDST.2021.102480.

41 A. Sosnik, J. Das Neves and B. Sarmento, Mucoadhesive polymers in the design of nano-drug delivery systems for administration by non-parenteral routes: A review, *Prog. Polym. Sci.*, 2014, **39**(12), 2030–2075, DOI: 10.1016/J.PROGPOLYMSCI.2014.07.010.

42 K. Netsomboon and A. Bernkop-Schnürch, Mucoadhesive vs. mucopenetrating particulate drug delivery, *Eur. J. Pharm. Biopharm.*, 2016, **98**, 76–89, DOI: 10.1016/J.EJPB.2015.11.003.

43 T. M. M. Ways, *et al.*, Mucus-penetrating nanoparticles based on chitosan grafted with various non-ionic polymers: Synthesis, structural characterisation and diffusion studies, *J. Colloid Interface Sci.*, 2022, **626**, 251–264, DOI: 10.1016/J.JCIS.2022.06.126.

44 N. Rajana, *et al.*, Targeted delivery and apoptosis induction of CDK-4/6 inhibitor loaded folic acid decorated lipid-polymer hybrid nanoparticles in breast cancer cells, *Int. J. Pharm.*, 2024, **651**, 123787, DOI: 10.1016/J.IJPHARM.2024.123787.

45 N. Rajana, *et al.*, Fabrication and characterization of teriflunomide-loaded chondroitin sulfate hybridized zein nanoparticles for the management of triple negative breast cancer, *Int. J. Biol. Macromol.*, 2025, **300**, 140316, DOI: 10.1016/J.IJBIOMAC.2025.140316.

46 Y. S. Pooja, N. Rajana, R. Yadav, L. T. Naraharisetti, C. Godugu and N. K. Mehra, Design, development, and evaluation of CDK-4/6 inhibitor loaded 4-carboxy phenyl boronic acid conjugated pH-sensitive chitosan lecithin nanoparticles in the management of breast cancer, *Int. J. Biol. Macromol.*, 2024, **258**, 128821, DOI: 10.1016/J.IJBIOMAC.2023.128821.

47 P. S. Chary, *et al.*, Enhancing breast cancer treatment: Comprehensive study of gefitinib-loaded poloxamer 407/TPGS mixed micelles through design, development, in-silico modelling, *In vitro* testing, and *Ex vivo* characterization, *Int. J. Pharm.*, 2024, **657**, 124109, DOI: 10.1016/J.IJPHARM.2024.124109.

48 S. Shaikh, P. S. Chary, O. Khan and N. K. Mehra, Development and evaluation of nilotinib-loaded Bovine Serum Albumin nanoparticles: *In vitro* and in-silico insights, *Int. J. Biol. Macromol.*, 2025, **308**, 142185, DOI: 10.1016/J.IJBIOMAC.2025.142185.

49 A. Mammella, V. Bhavana, P. S. Chary, U. Anuradha and N. K. Mehra, Modulation of chondroprotective hyaluronic acid and poloxamer gel with Ketoprofen loaded transethosomes: Quality by design-based optimization, characterization, and preclinical investigations in osteoarthritis, *Int. J. Biol. Macromol.*, 2024, **280**, 135919, DOI: 10.1016/J.IJBIOMAC.2024.135919.

50 N. U. Kumari, P. S. Chary, E. Pardhi and N. K. Mehra, Tailoring micellar nanocarriers for pemetrexed in breast cancer: design, fabrication and in vitro evaluation, *Nanomedicine*, 2024, **19**, 1145–1166, DOI: 10.2217/NNM-2024-0013.

51 P. S. Chary, *et al.*, Enhancing breast cancer treatment: Comprehensive study of gefitinib-loaded poloxamer 407/TPGS mixed micelles through design, development, in-silico modelling, *In vitro* testing, and *Ex vivo* characterization, *Int. J. Pharm.*, 2024, **657**, 124109, DOI: 10.1016/J.IJPHARM.2024.124109.

52 W. Zhou, *et al.*, Mucus-penetrating dendritic mesoporous silica nanoparticle loading drug nanocrystal clusters to enhance permeation and intestinal absorption, *Biomater. Sci.*, 2023, **11**(3), 1013–1030, DOI: 10.1039/D2BM01404A.

53 R. Albash, M. A. El-Nabarawi, H. Refai and A. A. Abdelbary, Tailoring of PEGylated bilosomes for promoting the transdermal delivery of olmesartan medoxomil: *in vitro* characterization, *ex vivo* permeation and *in vivo* assessment, *Int. J. Nanomed.*, 2019, **14**, 6555–6574, DOI: 10.2147/IJN.S213613.